Atmos. Chem. Phys. Discuss., 15, 12583–12616, 2015
www.atmos-chem-phys-discuss.net/15/12583/2015/
doi:10.5194/acpd-15-12583-2015
© Author(s) 2015. CC Attribution 3.0 License.

Atmospheric Chemistry and Physics Discussions

This discussion paper is/has been under review for the journal Atmospheric Chemistry and Physics (ACP). Please refer to the corresponding final paper in ACP if available.

Four-year long-path monitoring of ambient aerosol extinction at a central European urban site: dependence on relative humidity

A. Skupin, A. Ansmann, R. Engelmann, P. Seifert, and T. Müller

Leibniz Institute for Tropospheric Research, Permoserstraße 15, 04318 Leipzig, Germany

Received: 23 February 2015 – Accepted: 14 April 2015 – Published: 29 April 2015

Correspondence to: A. Skupin (skupin@tropos.de)

Published by Copernicus Publications on behalf of the European Geosciences Union.

Abstract

The ambient aerosol particle extinction coefficient is measured with the Spectral Aerosol Extinction Monitoring System (SÆMS) along a 2.84 km horizontal path at 30–50 m height above ground in the urban environment of Leipzig (51.3° N, 12.4° E), Germany, since 2009. The dependence of the particle extinction coefficient (wavelength range from 300–1000 nm) on relative humidity up to almost 100 % was investigated. The main results are presented. For the wavelength of 550 nm, the mean extinction enhancement factor was found to be 1.75 ± 0.4 for an increase of relative humidity from 40 to 80 %. The respective four-year mean extinction enhancement factor is 2.8 ± 0.6 for a relative-humidty increase from 40 to 95 %. A parameterization of the dependency of the urban particle extinction coefficient on relative humidity is presented. A mean hygroscopic exponent of 0.463 for the 2009–2012 period was determined. Based on a backward trajectory cluster analysis, the dependence of several aerosol optical properties for eight air flow regimes was investigated. Large differences were not found indicating that local pollution sources widely control the aerosol conditions over the urban site. The comparison of the SÆMS extinction coefficient statistics with respective statistics from ambient AERONET sun photometer observations yield good agreement. Also, time series of the particle extinction coefficient computed from in-situ-measured dry particle size distributions and humidity-corrected SÆMS extinction values (for 40 % relative humidity) were found in good overall consistency, which corroborates the applicability of the developed humidity parameterization scheme. The analysis of the spectral dependence of particle extinction (Ångström exponent) revealed an increase of the 390–881 nm Ångström exponent from, on average, 0.3 (at 30 % relative humidity) to 1.3 (at 95 % relative humidity) for the four-year period.

ACPD
15, 12583–12616, 2015

1 Introduction

The importance of atmospheric aerosols in the global climate system due to scattering and absorption of radiation and the influence on the formation of clouds is well known (Charlson and Heintzenberg, 1995; Heintzenberg and Charlson, 2009). However, a realistic consideration of atmospheric aerosols in climate models and the quantification of aerosol-related climate effects is a rather crucial task, not only because of the high horizontal, vertical, and temporal variability of aerosol concentrations, but also as a result of the highly variable microphysical and chemical properties of the occurring aerosols originating from many and rather different anthropogenic and natural sources. Furthermore, as a function of particle chemical composition, particle age, and state of aerosol mixture, aerosols can show a very different hygroscopic behavior (i.e., water uptake with increasing relative humidity), which further complicates the impact of aerosol particles on the Earth's radiation budget. There is a clear need for more field observations of ambient aerosol optical properties as a function of relative humidity from low (< 40 %) to very high values (> 95 %) to better describe aerosols in climate models as well as to better separate of aerosols and clouds in satellite remote sensing products. However, it is not a simple task to accurately determine the volume extinction coefficient for a given aerosol scenario without any manipulation of the aerosol system. Such a manipulation can not be avoided when aerosols are sampled and analyzed by means of in situ measurement techniques. Only remote sensing methods are able to avoid the disturbance of the aerosol conditions to be measured.

Only a few publications are available for particle growth in high-humidity environments with relative humidities up to almost 100 %, before cloud droplet activation begins (Arnulf et al., 1957; Goes, 1963; Elterman, 1964; Goes, 1964; Badayev et al., 1975; Stratmann et al., 2010; Liu et al., 2011; Chen et al., 2014). These efforts were partly based on controlled laboratory studies. Motivated by the need for more aerosol field observations with emphasis on undisturbed, but complex aerosol mixtures at ambient humidity conditions, we designed and setup the Spectral Aerosol Extinction Mon-

ACPD
15, 12583–12616, 2015

itoring System (SÆMS) (Skupin et al., 2014) which allows us to continuously monitor the wavelength spectrum of the particle extinction coefficient at a height of 30–50 m above ground between two towers which are 2.84 km apart from each other. The measurements cover all seasons of the year. Simultaneously, relative humidity and temperature are recorded at both towers at the height level of the aerosol extinction measurement path. The most interesting days for our study are those with a strong change in relative humidity, e.g., from nearly 100 % in the early morning to 30–40 % later on during the day and correspondingly strong changes in the particle extinction coefficient.

In our first article, we described the Spectral Aerosol Extinction Monitoring System (SÆMS) in detail (Skupin et al., 2014), discussed the quality and uncertainties of the observations, and presented case studies to show the potential of the newly designed remote sensing facility. In this article, we summarize the main findings of our long-term observations which cover the four-year period from January 2009 to December 2012. Besides the study of the dependence of particle extinction on relative humidity, we provide a general overview of the four-year statistics of particle extinction coefficients. We further compare the statistics with simultaneously performed Aerosol Robotic Network (AERONET) photometer observations and the optical properties derived from in situ measurements of the dry particle size distribution close to the SÆMS instrument. A similar study was presented by Müller et al. (2006) based on a short-term data set measured at the Leibniz Institute for Tropospheric Research (TROPOS) in March 2000. Here we expand the study and compare the entire year-2009 observations. The full set of analysis results can be found in Skupin (2014).

2 Instrumentation and data analysis methods

The long-term SÆMS aerosol measurements are performed in a suburban environment about 3 km northeast of the city center of Leipzig (51.3° N, 12.4° E, 120 m a.s.l.) in the eastern part of Germany since the beginning of 2009 (Skupin et al., 2014). Aerosol conditions are dominated by anthropogenic pollution (gas, oil, benzin, and coal burn-

ACPD
15, 12583–12616, 2015

ing, biomass-burning smoke, road dust) and natural continental aerosols (soil dust). The influence of marine particles can be regarded as low. SÆMS is installed in the roof laboratory of the main TROPOS building with a dome on top, and free view in all direction. The system is fully automated and allows us to measure the particle extinction spectrum from the from 300 to 1000 nm. SÆMS is part of the Leipzig Aerosol and Cloud Remote Observations System (LACROS) (Wandinger et al., 2012; Bühl et al., 2013), which includes European Aerosol Research Lidar Network (EARLINET) lidars, a Cloudnet station consisting of a ceilometer, cloud radar, and microwave radiometer (Illingworth et al., 2007), and the AERONET sun/sky photometer (Holben et al., 1998).

The measurement principle is illustrated in Fig. 1. The radiation beam of a broadband 450 W Xe-arc-high-pressure lamp is alternatively pointed to retroreflectors mounted at two towers at heights of 30 and 50 m above ground. The steering unit for light transmission and the receiving and detection units of SÆMS are mounted in the roof laboratory of TROPOS. The towers are 300 and 3140 m northeast of the TROPOS building. As explained in detail by Skupin et al. (2014) and Skupin (2014) the measurements allow us to determine the volume extinction coefficient $b_{p,e}$ of particles along the horizontal path of 2840 m between the two towers. Figure 2 shows all extinction measurements for the 2009–2012 period for three different wavelengths as a function of relative humidity. The relative humidity (RH) as well as the air temperature (T) are simultaneously measured close to the retroreflectors at the towers as well as on the roof of the TROPOS building. Figure 3 shows an example of a week-long time series of relative humidity, measured at the different sites. We use the total set of meteorological data (measured at all three locations) to check the homogeneity of the air mass along the SÆMS beam.

In this article, we concentrate on the influence of relative humidity on the optical properties, and briefly introduce several quantities used in this context. Following the notation of Skupin et al. (2014), the Ångström exponent (Ångstrom, 1964), which de-

ACPD
15, 12583–12616, 2015

scribes the spectral dependence of the extinction coefficient, is defined as

$$\alpha(\lambda_1, \lambda_2) = -\frac{\ln[b_{\mathrm{p,e}}(\lambda_1)/b_{\mathrm{p,e}}(\lambda_2)]}{\ln(\lambda_1/\lambda_2)} \quad (1)$$

with the particle extinction coefficient $b_{\mathrm{p,e}}(\lambda_N)$ for wavelength λ_N.

The particle extinction coefficient $b_{\mathrm{p,e}}(\lambda)$ increases with relative humidity. We consider this by introducing the humidity parameter f_1 with, e.g., $f_1 = 0.8$ for 80 % relative humidity. The so-called extinction enhancement factor $b^*_{f_1,f_0}(\lambda)$ is defined as:

$$b^*_{f_1,f_0}(\lambda) = \frac{b_{\mathrm{p,e}}(\lambda, f_1)}{b_{\mathrm{p,e}}(\lambda, f_0)} \quad (2)$$

which describes the increase of the particle extinction coefficient at $f_1 > f_0$ with respect to the dry-particle extinction coefficient at, e.g., $f_0 = 0.4$. Following Hänel (1984) with focus on anthropogenic pollution (mixture of urban haze and rural background aerosol), we can describe the dependence of particle extinction on ambient relative humidity conditions by means of:

$$b_{\mathrm{p,e}}(\lambda, f_1) = b_{\mathrm{p,e}}(\lambda, f_0 = 0)(1 - f_1)^{-\gamma}. \quad (3)$$

Hänel (1984) introduced an extension for the high humidity range ($0.7 < f_1 < 0.99$) as follows:

$$b_{\mathrm{p,e}}(\lambda, f_1) = b_{\mathrm{p,e}}(\lambda, f_0 = 0)c_1(\lambda)(1 - f_1)^{(-c_2)}. \quad (4)$$

The empirical parameters c_1 and c_2 are related to γ according to

$$\gamma = \left(c_2 - \frac{\ln c_1}{\ln 0.3}\right). \quad (5)$$

For urban aerosols, $c_1 = 0.7008$ and $c_2 = 0.7317$ for 550 nm so that $\gamma = 0.4364$ after Hänel (1984).

ACPD
15, 12583–12616, 2015

3 Results

3.1 Overview

Figure 4 provides an overview of the particle extinction conditions at Leipzig. Shown is the frequency distribution of measured 550 nm ambient extinction coefficients (top panel) and, for comparison, the extinction frequency distribution after normalization of all values to 0 % relative humidity (bottom panel) by using Eqs. (3) and (4) and appropriate input parameters c_1 and c_2 discussed below. The 2009–2012 mean values and standard deviations (SD) are $210 \pm 170\,\mathrm{M\,m^{-1}}$ for ambient conditions and $110 \pm 80\,\mathrm{M\,m^{-1}}$ for dry aerosol conditions. Thus the particle water content is responsible for roughly 50 % of particle extinction in the lowermost part of the troposphere at this urban site. Mattis et al. (2004) analyzed the Leipzig EARLINET Raman lidar observations conducted from 2000–2003, and found a mean extinction coefficient for 532 nm wavelength and ambient humidity conditions of $94 \pm 50\,\mathrm{M\,m^{-1}}$ in the upper part of the planetary boundary layer (PBL, above 1000 m height). Obviously, surface-near extinction values are a factor of 2 higher than at greater PBL heights.

3.2 Case studies

Days with a strong decrease in relative humidity during the morning hours or a strong increase in the evening served as the basis for our specific investigation of the influence of water uptake by particles on their optical properties. We sampled 143 days during the four-year period with a pronounced diurnal cycle in terms of relative humidity. Figure 5 presents two examples. Besides the influence of the relative humidity, changing air flow direction (long-range transport) and the daily evolution of the PBL can have a sensitive impact on the surface-near particle extinction coefficient. The backward trajectories (HYbrid Single-Particle Lagrangian Integrated Trajectory Model, HYSPLIT, http://www.arl.noaa.gov/HYSPLIT.php) (Draxler and Hess, 1997, 1998; Draxler, 1999) indicate almost constant long-range aerosol transport conditions during the shown

ACPD
15, 12583–12616, 2015

measurement periods. The particle optical depth at 500 nm as observed with the AERONET photometer was around 0.1 ± 0.04 over the whole day until 16:00 UTC on 20 August, and thus confirmed the almost constant aerosol conditions during time period shown in Fig. 5b.

According to the lidar observation on 20 August 2009, the PBL development (growth of the PBL height with time) was found to influence the aerosol extinction properties close to the surface not before about 11:30 UTC. As a general result of the 2009–2012 lidar observations we found that the diurnal PBL evolution only affects the surface-near aerosol concentration to a significant amount when the growing PBL grasps into the clean free troposphere so that any further increase in PBL depth reduces the aerosol concentration in the entire PBL by downward mixing of clean free tropospheric air. As long as the convectively active PBL is developing into the polluted residual layer ontop of the growing, but shallow PBL, the impact of the PBL development on the measured surface-near extinction coefficient was usually found to be low. The steady decrease of the extinction coefficient from 11:30 to 15:00 UTC on 20 August 2009 in Fig. 5b is the result of the growing PBL and corresponding downward mixing of clean air from the free troposphere. The PBL depth increased from 1300 to 1900 m (30 % increase). This is directly reflected in the decrease of the extinction coefficient from values around 0.2 to values around 0.14, while the relative humidity decreased from 53 to 48 % only.

On 27 August 2009, cloudy weather prevailed. The trajectories in Fig. 5d show a constant air flow from southwest. The lidar detected a deep, aged aerosol layer (residual layer) up to 2 km height in the morning. The layer depth increased to 2.5 km height until the evening, mainly by advection of even more polluted air from France. The AERONET photometer recorded an optical depth of 0.2 ± 0.05 for 500 nm throughout the day, indicating a polluted, aged European air mass. A pronounced PBL development was absent on that day. Thus the decrease of the particle extinction coefficient was widely controlled by the strongly decreasing relative humidity. The humidity was close to 100 % in the early morning around 03:30 UTC and decreased to almost 35 % in the afternoon around 13:30 UTC. The correlation between the simultaneously measured relative hu-

ACPD
15, 12583–12616, 2015

midity and particle extinction coefficient for the two different days is shown in Fig. 5c and f. Curve fitting (assuming a relative-humidity dependence according to Eqs. 3 and 4) reveals the values for c_1 and c_2, and γ as given in Fig. 5c and f. For the pronounced relative-humidity dependence on 27 August 2009, the parameter set is quite similar to the one for urban haze after Hänel (1984). For 27 August 2009, we obtain for the exponent $\gamma = 0.502$ after Eq. (5). Hänel (1984) found $\gamma = 0.4364$.

3.3 Extinction enhancement factor

The main statistical results of the analysis of all 143 days with pronounced diurnal cycle regarding relative humidity are summarized in Fig. 6. For each of the 143 days, the optimum curve after Eqs. (3) and (4) and the corresponding values for c_1, c_2, and γ were determined. From these data sets, the mean values $\overline{c_1}$, $\overline{c_2}$, and $\overline{\gamma}$, and the corresponding SD δc_1, δc_2, and $\delta\gamma$ as presented in Fig. 6 were calculated. The curve for the mean enhancement factor (blue curve in Fig. 6) is obtained with Eq. (3) and the mean value $\overline{\gamma}$. The upper and lower boundaries of the gray-shaded area in Fig. 6 are obtained by using $\overline{\gamma} + \delta\gamma$ (upper boundary) and $\overline{\gamma} - \delta\gamma$ (lower boundary) in Eq. (3). The close agreement of the blue curve with the green curve for urban haze after Hänel (1984) in Fig. 6 corroborates the high quality and reliability of our long-term observations. More case studies and more details to the parameterization efforts can be found in Skupin (2014).

3.4 Extinction coefficient and enhancement factor for different air flow conditions

In order to investigate to what extend regional and long-range transport of aerosols influenced our measurements we performed an extended cluster analysis based on HYSPLIT backward trajectories for all selected observations. We considered 18 000 individual SÆMS observations performed in the years 2009–2012 in this study. The cluster analysis revealed eight different air flow regimes. Figure 7 presents an overview

ACPD
15, 12583–12616, 2015

of the surface-near particle extinction conditions over Leipzig for different airflow directions. In Fig. 7a, mean values and SD of the particle extinction coefficient for ambient conditions are given. Note the two westwind clusters (for strong westerly winds and for slow air mass transport from the west). Figure 7b shows the cluster mean extinction values after normalization to 0 % relative humidity by using cluster mean values for c_1 and c_2. In Fig. 7c, the dry particle extinction coefficients are given for the individual years from 2009–2012.

The main findings can be summarized as follows: after removing of the humidity effect on light extinction, the extinction coefficients are generally a factor of 2 lower then for ambient conditions, disregarding specific airflow conditions. The largest extinction coefficients with a mean value of 0.23 km^{-1} (0.11 km^{-1} for dry particles) were observed when the air masses were advected from easterly directions, i.e., from the eastern parts of Leipzig (with the highway A14), from the most eastern parts of Germany, Poland, Ukraine, and polluted southeastern European regions. The lowest extinction coefficients (about a factor of 2 lower then the east-cluster values) were observed during situations with fast westerly air mass transport. Pronounced contributions to particle extinction by the Leipzig city center (clusters 5–7 in Fig. 7c) were not found. On average, the surface-near extinction coefficients are about 0.17 km^{-1} (0.08 km^{-1} for dry particles) with an only weak dependence on the airflow conditions. Particle extinction conditions at our SÆMS measurement site were obviously widely controlled by local and regional aerosol sources and, only to a second order, by long-range aerosol advection.

The year-by-year statistics of dry particle extinction coefficients in Fig. 7c corroborate this impression. Air masses advected from the east show the highest extinction values in each of the four years and the variations of the individual cluster-mean extinction values around the overall mean are in the 10–20 % range (except for the east cluster). However, year-by-year differences are also obvious. The comparably large 2010 extinction values are caused by strong construction activties in the eastern parts of the Leipzig greater area. Highway construction works covered the whole year to extend

ACPD
15, 12583–12616, 2015

the four-lane highway A14 to a six-lane road. In contrast, in 2011 new traffic emission reducing regularizations were brought into operation and may have caused the overall low particle extinction values observed in 2012. There is almost no difference in the precipitation amount for the years 2011 and 2012 which could explain a potentially stronger wash out effect in 2012 and frequent cleaning of the streets (and reduced road dust effects).

Figure 8 provides an overview of the mean particle enhancement factor (and corresponding SD) for the different airflow clusters. The shown mean values and SD of the ratio of particle extinction at 80 or 95 % relative humidity to the one at 40 % relative humidity were calculated from the available individual days with strong humidity variability for each of the eight air flow regimes separately. Nine (south cluster) to 29 days (northwest cluster) were available for the cluster-related investigations. As can be seen in Fig. 8, large differences between the clusters were not found. The 80-to-40 % extinction growth factor was 1.75 ± 0.4, on average with variations between the clusters mean values of the order of 0.1. Stronger differences between the clusters were found for the 95-to-40 % extinction growth factors. The largest value of 3.5 was observed for northerly air flows with the comparably largest influence of marine particles (at comparably low levels of pollution advection from the Baltic Sea and Scandinavia). The lowest growth factor of 2.3 was found for the south-wind cluster with a high amount of anthropogenic less hygroscopic pollution particles. On average, the 95-to-40 % extinction growth factors was 2.8 ± 0.6.

Figure 9 presents the cluster-mean γ values which were calculated from the individual c_1 and c_2 values by means of Eq. (5) for the individual days. Higher γ values reaching almost 0.6 and indicating more hygroscopic particles were found for the north and east clusters, whereas the lowest values around 0.4 were observed when the air was advected from the west or northeast. γ is closely correlated with the 80-to-40 % extinction growth factor and takes values of around 0.4, 0.5, and 0.6 for growth factors around 1.55, 1.7, and 1.85, respectively.

ACPD
15, 12583–12616, 2015

Table 1 provides literature values of the extinction growth factors for comparison. Values between 1.1 and 3.3 have been published for the 500–550 nm wavelength range. For biomass burning aerosol or background (rural) particles extinction growth factors as low as 1.0–1.2 were found. For polluted continental areas the growth factors accumulate from 1.6–2.0, and for marine particles values above 3.0 are observed. Our observations fit well into the larger frame of observed growth factors and adds new values for the high humidity range (95-to-40 % growth factors).

3.5 Extinction coefficient statistics: comparison of SÆMS-, AERONET-, and in situ observations

In Fig. 10, we compare our SÆMS measurements for a time period of five days in September 2009 with particle extinction coefficients at 550 nm derived from ground-based in situ measurements of the dry particle size distribution (Birmili et al., 2009). Such a comparison was already successfully performed for a ten-day period in March 2000 (Müller et al., 2006), with a similar apparatus as SÆMS but by using a very short optical path in the vicinity of the in situ measurement stations. A successful comparison between in situ aerosol observations on the roof of the TROPOS building and the SÆMS observations along the 2.8 km path was also shown in Fig. 8 in Skupin et al. (2014) for 3 May 2009.

The in situ extinction coefficients are computed from the measured size distributions of dried particles, i.e., for particle size distribution measured at relative humidities around 30 %. A so-called PM_{10} inlet is used so that very coarse particles with diameters larger than about 10 µm are not measured. The particle extinction coefficient was calculated by means of a Mie scattering code based on Bohren and Huffman (1983) as described in Skupin (2014). The real part of the refractive index was set to a constant value of 1.53 (typical value for urban haze). Absorption by particles was considered by assuming an imaginary part of 0.01i.

As can be seen, a good overall agreement between the in situ and SÆMS dry extinction time series (black and red curves) is obtained. The 2009 mean (±SD) and me-

ACPD
15, 12583–12616, 2015

dian dry particle extinction coefficients are $0.061 \pm 0.055\,km^{-1}$ and $0.046\,km^{-1}$ (in situ), respectively, and $0.073 \pm 0.036\,km^{-1}$ and $0.065\,km^{-1}$ (SÆMS, dry), respectively. The humidity-corrected SÆMS extinction coefficients in Fig. 10 are calculated from the ambient SÆMS extinction values by using the extinction enhancement parameterization shown in Fig. 6. The good agreement between the black and red curve corroborates the usefulness of the developed parameterization.

The strong impact of relative humidity on particle extinction (SÆMS, ambient) is nicely illustrated in Fig. 10. During the gray-shaded time periods from 13:00–17:00 UTC, when the PBL is well mixed at sunny days (days 267–269 in Fig. 10), the relative humidity and particle extinction take their daily minimum. During the afternoon hours, the PBL has the largest vertical extent which contributes to the observed low extinction values around 15:00 UTC. The systematically lower in situ extinction coefficients on these sunny days compared to the SÆMS (dry) values may be partly caused by the used constant refractive index which is probably not appropriate for all aerosol conditions throughout the day, especially not when aged particles (after long-range transport) are mixed down from higher altitudes and partly substitute the less aged urban haze close to the ground. The humidity correction may be also not valid at all for the aerosol conditions found during the convectively active period. Furthermore, we compare point measurements with long path measurements 300–3140 m apart from the PM_{10} inlet. TROPOS is part of an area with complex urban building structure, whereas the optical path of SÆMS crosses areas with much less buildings, even areas without any building, and is parallel to several large motorways and crosses the A14 highway.

In Fig. 11, extinction distributions derived from 2009 AERONET sun photometer and SÆMS (ambient) measurements are compared. The shown distribution curves are optimum fits to the respective frequency-of-occurrence distributions of measured and derived extinction coefficients. As before, we considered only data measured in the afternoon from 13:00 to 17:00 UTC, when the probability is highest that the PBL is well mixed. In the case of the AERONET observations, the extinction distribution curve shows PBL mean extinction values (vertical column mean values). All measured

ACPD
15, 12583–12616, 2015

500 nm aerosol particle optical thickness (AOT) values were divided by the respective PBL height, obtained from numerical weather prediction data (GDAS: global assimilation system, http://www.arl.noaa.gov/gdas.php) (Kanamitsu, 1989), before the calculation of the frequency-of-occurrence distribution. At well-mixed conditions the PBL mean particle extinction coefficient is closest to the extinction value measured with SÆMS during the day.

As can be seen in Fig. 11, a rather good agreement between the SÆMS (ambient) and the AERONET observations is found. A systematic overestimation of the PBL mean extinction value must be kept in consideration in the interpretation of the AERONET observations, because, on average, 20 % of the AOT is caused by particles in the free troposphere (Mattis et al., 2004). We did also not correct for a wavelength dependence of particle extinction. On average, 550 nm extinction coefficients are about 10–15 % lower than the values at 500 nm.

For comparison, also the distribution of dry extinction coefficients as obtained from the SÆMS observations after humidity correction and the extinction distribution calculated from the in-situ-measured dry particle size distributions are shown for the specific 13:00–17:00 UTC time period. The possible reasons for the found deviations between the two dry extinction frequency-of-occurrence distributions were discussed above.

3.6 Extinction wavelength dependence as a function of relative humidity

Finally, we briefly summarize the influence of a relative-humidity increase on the spectral slope of the particle extinction coefficient for the wavelength range from 390 to 881 nm. Figure 12 shows a steady increase of the Ångström exponent (see Eq. 1) with increasing relative humidity for the entire spectrum from 390–881 nm and a decrease for the short wavelength range (390–440 nm). The figure is based on all measurements in 2009 and 2010. The reason for the increase of the 390–881 nm Ångström exponent and the decrease of the 390–440 nm Ångström exponent is shown in Fig. 13. A strong increase of the 390 nm particle extinction coefficient was observed with increasing relative humidity, an even stronger increase was observed at 440 nm, whereas no or

ACPD
15, 12583–12616, 2015

even a decreasing trend of the extinction strength with increasing relative humidity at 881 nm. A strong water-uptake effect for fine-mode particles with radius < 100 nm can explain the strong increase of the extinction coefficient at the shorter wavelengths as our Mie scattering calculations indicate. The impact of fine-mode particles on the extinction coefficient at 881 nm is low. In contrast, the coarse particles (road dust and others) obviously do not grow significantly by water-uptake so that the extinction coefficient at 881 nm, dominated by large particles, remains low for all ambient humidity conditions. Consequently, the overall 390–881 nm Ångström exponent increases with relative humidity.

Significantly different Ångström exponents for the eight air-flow classes were not observed pointing again to the dominating influence of local and regional pollution on the aerosol conditions at our field site. It is finally worthwhile to mention that the mean value and SD for the 440–881 nm Ångström exponent for the years of 2009 and 2010 is 1.55 ± 0.42 in the case of the AERONET column measurements. In contrast the 390–881 nm SÆMS Ångström exponents show a mean value of 0.91 ± 0.68.0 (Skupin, 2014) for the 2009–2010 period, a clear indication of the strong impact of coarse particles on the SÆMS observations.

4 Conclusions

For the first time, a long-term study of the surface-near particle extinction coefficient at undisturbed aerosol and humidity conditions at a central European urban site has been presented. The dependence of particle extinction on relative humidity could be studied from 20 to almost 100 % relative humidity. For the wavelength of 550 nm, the mean extinction enhancement factor was found to be 1.75 ± 0.4 (for a humidity increase from 40 to 80 %) and 2.8 ± 0.6 for a relative humidity increase from 40 to 95 %. A parameterization of the humidity dependence of the particle extinction coefficient was derived. A mean hygroscopic exponent γ of 0.463 for the 2009–2012 period was retrieved. Based on an extended backward trajectory cluster analysis, a weak depen-

ACPD
15, 12583–12616, 2015

dence of the particle optical properties (AOT, extinction enhancement factor, Ångström exponent) from the air flow condition has been observed. Locally produced aerosol particles widely controlled the measured ambient aerosol optical properties.

As an outlook, a mobile SÆMS (based on a simplified setup with, e.g., three diode lasers as radiation sources operating around 400, 550, and 850 nm) would be desirable to study basic ambient aerosol conditions at very different places (rural areas, background stations, marine environments, regions influenced by desert dust). However, to investigate the dependence of particle extinction on relative humidity, strong ambient humidity changes must occur, which may not be observable on islands or desert sites.

Acknowledgements. We thank the Deutsche Forschungsgemeinschaft for funding under grant HE 939/30-1 and AN 258/18-1. In situ particle size distributions at Leipzig-TROPOS were provided by Wolfram Birmili and Kay Weinhold. These measurements within the German Ultrafine Aerosol Network (GUAN) were supported by the German Federal Environment Ministry (BMU) grant F&E 370343200 (German title: "Erfassung der Zahl feiner und ultrafeiner Partikel in der Außenluft"). We also thank K. Flachowsky and R. Dubois for providing the meteorological data.

References

Adam, M., Putaud, J. P., Martins dos Santos, S., Dell'Acqua, A., and Gruening, C.: Aerosol hygroscopicity at a regional background site (Ispra) in Northern Italy, Atmos. Chem. Phys., 12, 5703–5717, doi:10.5194/acp-12-5703-2012, 2012. 12603

Ångstrom, A.: The parameters of atmospheric turbidity, Tellus, 16, 64–75, 1964. 12587

Arnulf, A., Bricard, J., Cure, E., and Veret, C.: Transmission by haze and fog in the spectral region 0.35 to 10 microns, J. Opt. Soc. Am., 47, 491–498, 1957. 12585

Badayev, V. V., Georgiyevskiy, Y. S., and Pirogov, S. M.: Aerosol extinction in the spectral range 0.25–2.2 µm, Izv., Atmos. Oceanic Phys., 11, 522–536, 1975. 12585

Birmili, W., Weinhold, K., Nordmann, S., Wiedensohler, A., Spindler, G., Müller, K., Herrmann, H., Gnauk, T., Pitz, M., Cyrys, J., Flentje, H., Nickel, C., Kuhlbusch, T., Löschau, G., Haase, D., Meinhardt, F., Schwerin, A., Ries, L., and Wirtz, K.: Atmospheric aerosol measurements in the German Ultrafine Aerosol Network (GUAN): Part 1 – soot and particle number size distributions, Gefahrst. Reinhalt L., 69, 137–145, 2009. 12594

ACPD
15, 12583–12616, 2015

Bohren, C. F. and Huffman, D. R.: Absorption and Scattering of Light by Small Particles, Wiley, New York, 1983. 12594

Bühl, J., Ansmann, A., Seifert, P., Baars, H., and Engelmann, R.: Toward a quantitative characterization of heterogeneous ice formation with lidar/radar: comparison of CALIPSO/CloudSat with ground-based observations, Geophys. Res. Lett., 40, 4404–4408, doi:10.1002/grl.50792, 2013. 12587

Carrico, C. M., Rood, M. J., Ogren, J. A., Neusüß, C., Wiedensohler, A., and Heintzenberg, J.: Aerosol optical properties at Sagres, Portugal during ACE-2, Tellus B, 52, 694–715, doi:10.1034/j.1600-0889.2000.00049.x, 2000. 12603

Charlson, R. and Heintzenberg, J.: Aerosol Forcing of Climate, Wiley, Chichester, 1995. 12585

Chen, J., Zhao, C. S., Ma, N., and Yan, P.: Aerosol hygroscopicity parameter derived from the light scattering enhancement factor measurements in the North China Plain, Atmos. Chem. Phys., 14, 8105–8118, doi:10.5194/acp-14-8105-2014, 2014. 12585, 12603

Draxler, R. R.: HYSPLIT4 user's guide, NOAA Tech. Memo. ERL ARL–230, NOAA Air Resources Laboratory, Silver Spring, MD, 1999. 12589

Draxler, R. R. and Hess, G. D.: Description of the HYSPLIT4 modeling system, NOAA Tech. Memo. ERL ARL–224, NOAA Air Resources Laboratory, Silver Spring, MD, 1997. 12589

Draxler, R. R. and Hess, G. D.: An overview of the HYSPLIT4 modeling system of trajectories, dispersion, and deposition, Aust. Meteorol. Mag., 47, 295–308, 1998. 12589

Elterman, L.: Atmospheric attenuation model, 1964, in the ultraviolet, visible, and infrared regions for altitudes to 50 km, Env. Res. Papers No. 46, Optical Physics Laboratory Project 7670, Air Force Cambridge Research Laboratories, Office of Aerospace Research, United States Air Force, L. G. Hanscom Field, Bedford, Mass., 40 pp., 1964. 12585

Fierz-Schmidhauser, R., Zieger, P., Gysel, M., Kammermann, L., DeCarlo, P. F., Baltensperger, U., and Weingartner, E.: Measured and predicted aerosol light scattering enhancement factors at the high alpine site Jungfraujoch, Atmos. Chem. Phys., 10, 2319–2333, doi:10.5194/acp-10-2319-2010, 2010. 12603

Goes, O. W.: Registrierung der Durchlässigkeit in verschiedenen Spektralbereichen in der Atmosphäre. 1. Teil, Contrib. Atmos. Phys., 36, 127–147, 1963. 12585

Goes, O. W.: Registrierung der Durchlässigkeit in verschiedenen Spektralbereichen in der Atmosphäre, 2. Teil, Contrib. Atmos. Phys., 37, 119–131, 1964. 12585

ACPD
15, 12583–12616, 2015

Hänel, G.: Parametrization of the influence of relative humidity on optical aerosol properties, in: Aerosols and their Climatic Effects, edited by: Gerber, H. and Deepak, A., A. Deepak, Hampton, Virgina, 117–122, 1984. 12588, 12591, 12609

Heintzenberg, J. and Charlson, R. J.: Clouds in the Perturbed Climate System: Their Relationship to Energy Balance, Atmospheric Dynamics, and Precipitation, MIT Press, Cambridge, Mass., 2009. 12585

Holben, B. N., Eck, T. F., Slutsker, I., Tanre, D., Buis, J. P., Setzer, A., Vermote, E., Reagan, J. A., Kaufman, Y. J., Nakajima, T., Lavenu, F., Jankowiak, I., and Smirnov, A.: AERONET – a federated instrument network and data archive for aerosol characterization, Remote Sens. Environ., 66, 1–16, 1998. 12587

Illingworth, A. J., Hogan, R. J., O'Connor, E. J., Bouniol, D., Delanoe, J., Pelon, J., Protat, A., Brooks, M. E., Gaussiat, N., Wilson, D. R., Donovan, D. P., Klein Baltink, H., van Zadelhoff, G.-J., Eastment, J. D., Goddard, J. W. F., Wrench, C. L., Haeffelin, M., Krasnov, O. A., Russchenberg, H. W. J., Piriou, J.-M., Vinit, F., Seifert, A., Tompkins, A. M., and Willen. J.: CLOUDNET: continuos evaluation of cloud profiles in seven operational models using ground-based observations, B. Am. Meteorol. Soc., 88, 883–898, doi:10.1175/BAMS-88-6-883, 2007. 12587

Im, J.-S., Saxena, V. K., and Wenny, B. N.: An assessment of hygroscopic growth factors for aerosols in the surface boundary layer for computing direct radiative forcing, J. Geophys. Res., 106, 20213–20224, doi:10.1029/2000JD000152, 2001. 12603

Kanamitsu, M.: Description of the NMC global data assimilation and forecast system, Weather Forecast., 4, 335–342, 1989. 12596

Kim, J., Yoon, S.-C., Jefferson, A., and Kim, S.: Aerosol hygroscopic properties during Asian dust, pollution, and biomass burning episodes at Gosan, Korea in April 2001, Atmos. Environ., 40, 1550–1560, 2006. 12603

Kotchenruther, R. A. and Hobbs, P. V.: Humidification factors of aerosols from biomass burning in Brazil, J. Geophys. Res., 103, 32081–32089, 1998. 12603

Kotchenruther, R. A., Hobbs, P. V., and Hegg, D. A.: Humidification factors for atmospheric aerosols off the mid-Atlantic coast of the United States, J. Geophys. Res., 104, 2239–2251, 1999. 12603

Liu, P. F., Zhao, C. S., Göbel, T., Hallbauer, E., Nowak, A., Ran, L., Xu, W. Y., Deng, Z. Z., Ma, N., Mildenberger, K., Henning, S., Stratmann, F., and Wiedensohler, A.: Hygroscopic properties of aerosol particles at high relative humidity and their diurnal variations in the North China Plain, Atmos. Chem. Phys., 11, 3479–3494, doi:10.5194/acp-11-3479-2011, 2011. 12585

ACPD
15, 12583–12616, 2015

Liu, X., Gu, J., Li, Y., Cheng, Y., Qu, Y., Han, T., Wang, J., Tian, H., Chen, J., and Zhang, Y.: Increase of aerosol scattering by hygroscopic growth: observation, modeling, and implications on visibility, Atmos. Res., 132–133, 91–101, doi:10.1016/j.atmosres.2013.04.007, 2013. 12603

Magi, B. I. and Hobbs, P. V.: Effects of humidity on aerosols in southern Africa during the biomass burning season, J. Geophys. Res., 108, 8495, doi:10.1029/2002JD002144, 2003. 12603

Mattis, I., Ansmann, A., Müller, D., Wandinger, U., and Althausen, D.: Multiyear aerosol observations with dual-wavelength Raman lidar in the framework of EARLINET, J. Geophys. Res., 109, D13203, doi:10.1029/2004JD004600, 2004. 12589, 12596

Müller, T., Müller, D., and Dubois, R.: Particle extinction measured at ambient conditions with differential optical absorption spectroscopy. 2. Closure study., Appl. Optics, 45, 2295–2305, 2006. 12586, 12594, 12603

Sheridan, P. J., Jefferson, A., and Ogren, J. A.: Spatial variability of submicrometer aerosol radiative properties over the Indian Ocean during INDOEX, J. Geophys. Res., 107, 8011, doi:10.1029/2000JD000166, 2002. 12603

Skupin, A.: Optische und mikrophysikalische Charakterisierung von urbanem Aerosol bei (hoher) Umgebungsfeuchte, optical and microphysical characterization of urban aerosol at (high) ambient relative humidity, Ph.D. thesis, 176 pp., Universität Leipzig, and Leibniz Institute for Tropospheric Research, Leipzig, Germany, 2014. 12586, 12587, 12591, 12594, 12597

Skupin, A., Ansmann, A., Engelmann, R., Baars, H., and Müller, T.: The Spectral Aerosol Extinction Monitoring System (SÆMS): setup, observational products, and comparisons, Atmos. Meas. Tech., 7, 701–712, doi:10.5194/amt-7-701-2014, 2014. 12586, 12587, 12594

Stratmann, F., Bilde, M., Dusek, U., Frank, G. P., Hennig, T., Henning, S., Kiendler-Scharr, A., Kiselev, A., Kristensson, A., Lieberwirth, I., Mentel, T. F., Pöschl, U., Rose, D., Schneider, J., Snider, J. R., Tillmann, R., Walter, S., and Wex, H.: Examination of laboratory-generated coated soot particles: an overview of the LACIS Experiment in November (LExNo) campaign, J. Geophys. Res., 115, D11203, doi:10.1029/2009JD012628, 2010. 12585

Wandinger, U., Seifert, P., Wagner, J., Engelmann, R., Bühl, J., Schmidt, J., Heese, B., Baars, H., Hiebsch, A., Kanitz, T., Althausen, D., and Ansmann, A.: Integrated remote-sensing techniques to study aerosols, clouds, and their interaction, in: Proceedings of the

ACPD
15, 12583–12616, 2015

26th Internation Laser Radar Conference (ILRC 2012), edited by: Papayannis, A., Balis, D., and Amiridis, V., Porto Heli, Greece, 25–29 June 2012, vol. 1, 395–398, 2012. 12587

Zieger, P., Fierz-Schmidhauser, R., Gysel, M., Ström, J., Henne, S., Yttri, K. E., Baltensperger, U., and Weingartner, E.: Effects of relative humidity on aerosol light scattering in the Arctic, Atmos. Chem. Phys., 10, 3875–3890, doi:10.5194/acp-10-3875-2010, 2010. 12603

Zieger, P., Fierz-Schmidhauser, R., Poulain, L., Müller, T., Birmili, W., Spindler, G., Wiedensohler, A., Baltensperger, U., and Weingartner, E.: Influence of water uptake on the aerosol particle light scattering coefficients of the Central European aerosol, Tellus B, 66, 22716, doi:10.3402/tellusb.v66.22716, 2014. 12603

ACPD
15, 12583–12616, 2015

Table 1. Overview of published particle extinction enhancement factors based on extinction values measured at different values of relative humidity RH (%).

Region	Aerosol type	RH (wet/dry)	Enhancement factor	Reference
Brazil	biomass burning	80/30	1.01–1.51	Kotchenruther and Hobbs (1998)
USA	urban/industrial	80/30	1.81–2.3	Kotchenruther et al. (1999)
Portugal	anthropogen	82/27	1.46	Carrico et al. (2000)
India	biomass burning or dust	85/40	1.58	Sheridan et al. (2002)
Africa	biomass burning	80/30	1.42–2.07	Magi and Hobbs (2003)
Korea	dust	85/20	2.00	Kim et al. (2006)
Suisse	rural	85/20	1.21–3.3	Fierz-Schmidhauser et al. (2010)
Norge	marine	85/20	3.24	Zieger et al. (2010)
Italy	rural	90/0	2.1	Adam et al. (2012)
United States	polluted continental, marine-pollution mixtures	80/30	1.6	Im et al. (2001)
China	urban	80/40	1.9	Liu et al. (2013)
China	polluted continental	90/40	1.93	Chen et al. (2014)
Germany	polluted continental	85/10	1.2–3.6	Zieger et al. (2014)
Germany	urban	80/40	1.86	Müller et al. (2006)
Germany	urban	80/0	2.12	Müller et al. (2006)
Germany	urban	80/40	1.37–1.99	this work
Germany	urban	95/40	2.35–3.49	this work

ACPD
15, 12583–12616, 2015

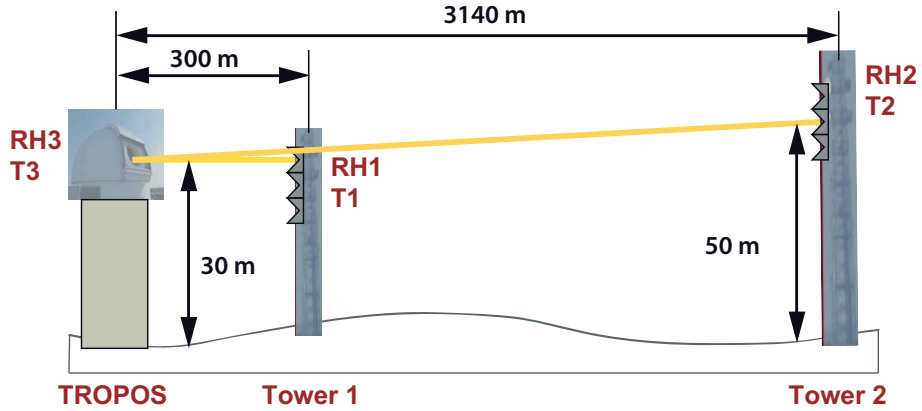

Figure 1. Sketch of the SÆMS measurement configuration. A light beam is transmitted at TROPOS and direct to a retroreflector array mounted at Tower 1 for several minutes. Afterwards the beam is moved to the second retroreflector array at Tower 2 for several minutes, followed by the next round in which the beam is again directed to Tower 1, and so on. Particle extinction is derived from the Tower 1 and Tower 2 long-path transmission observations, and thus is related to an almost horizontal path of 2840 m at a height of 30–50 m above ground. The aerosol particle extinction measurements are set into context with meteorological observations of temperature (T) and relative humidity (RH) which are measured at the roof of TROPOS (T3, RH3) and close to the retroreflectors at Tower 1 (RH1, T1) and Tower 2 (RH2, T2).

ACPD
15, 12583–12616, 2015

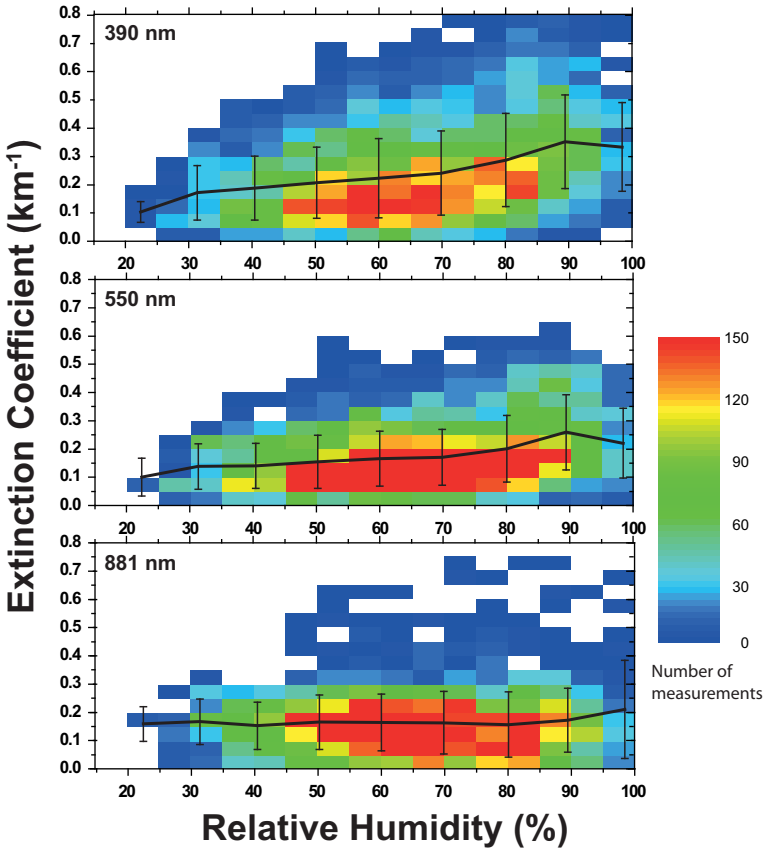

Figure 2. Measured particle extinction coefficients for the wavelengths of 390 nm (top), 550 nm (center), and 881 nm (bottom) as a function of relative humidity. The color scale indicates how frequently a given extinction coefficient was measured during the 2009–2012 period. Mean values (bold lines) of extinction coefficients and corresponding SD (vertical bars) are shown for 10 % humidity intervals.

ACPD
15, 12583–12616, 2015

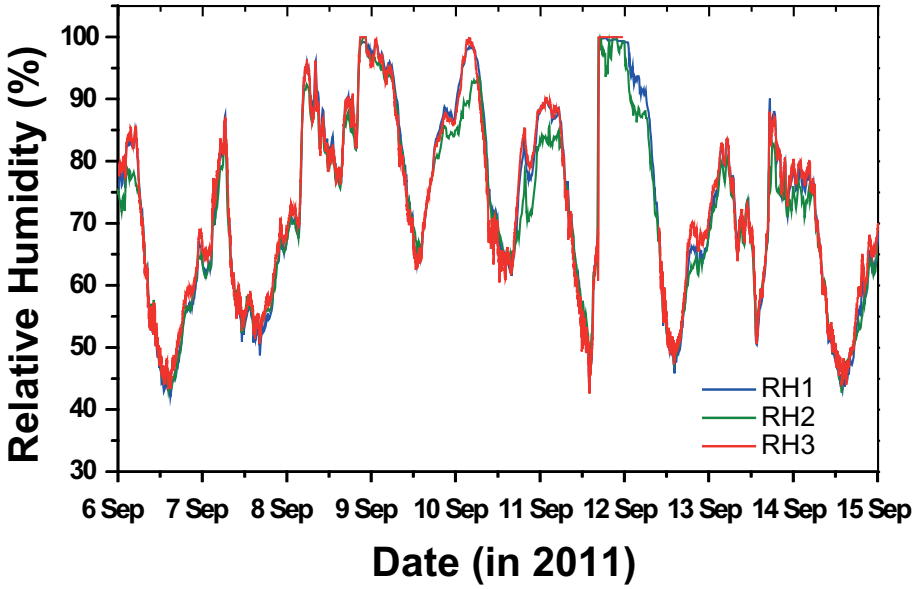

Figure 3. Example of the three-point relative humidity observation (over 9 days) with humidity sensors on top of the TROPOS building and at the two towers (see Fig. 1).

ACPD
15, 12583–12616, 2015

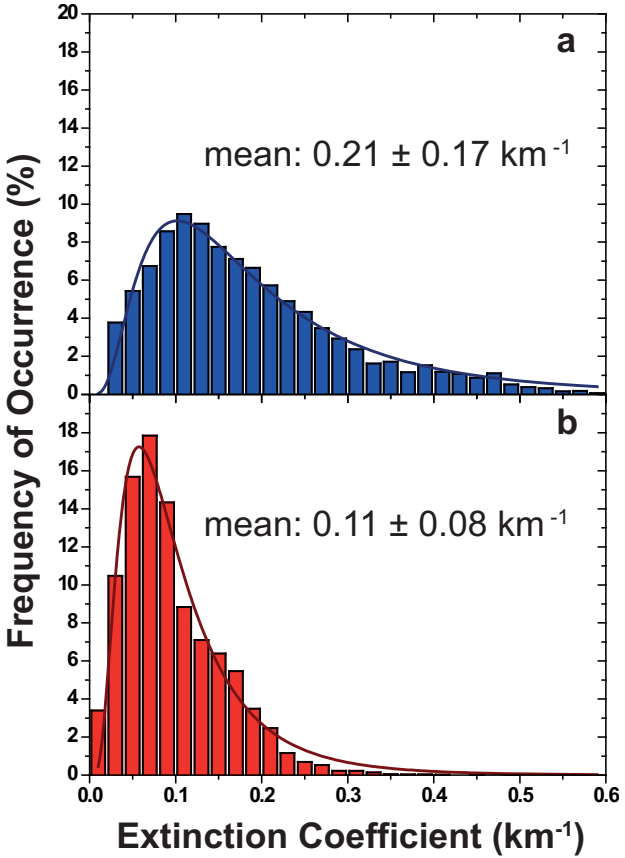

Figure 4. (a) Frequency distribution of ambient 550 nm particle extinction coefficient observed with SÆMS at Leipzig from 2009–2012, **(b)** same distribution after correction of the particle water uptake effect, i.e., after normalization of all values to 0 % relative humidity by means of Eqs. (3) and (4) with parameters for urban aerosol derived from the four-year SÆMS study. 2009–2012 mean values and respective SD are given as numbers.

ACPD
15, 12583–12616, 2015

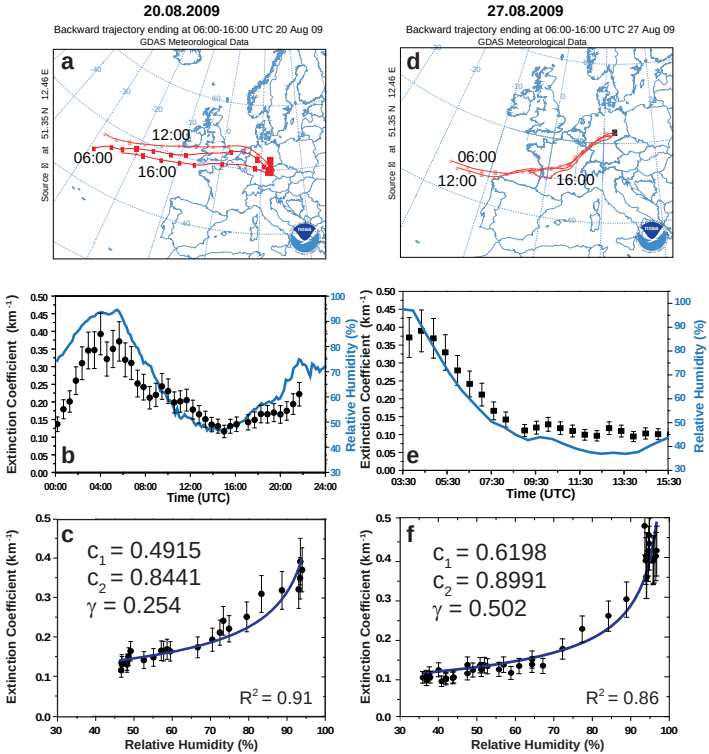

Figure 5. SÆMS observations on (left) 20 August 2009 and (right) 27 August 2009. Almost constant horizontal transport of polluted air from westerly to southwesterly directions is indicated by 4-day HYSPLIT backward trajectories (**a**, **d**, arrival height of 500 m). The temporal variation of the 550 nm particle extinction coefficient with relative humidity is shown in **(b)** for 20 August 2009 and in **(e)** for 27 August 2009, and the corresponding relationship between ambient extinction coefficient and relative humidity is presented in (**c** and **f**). The curves fitted to the data points in (**c** and **f**) are obtained with Eqs. (3) and (4) and the given values of c_1 and c_2. γ follows from Eq. (5). The coefficient of determination R^2 for each fit is given as number.

ACPD
15, 12583–12616, 2015

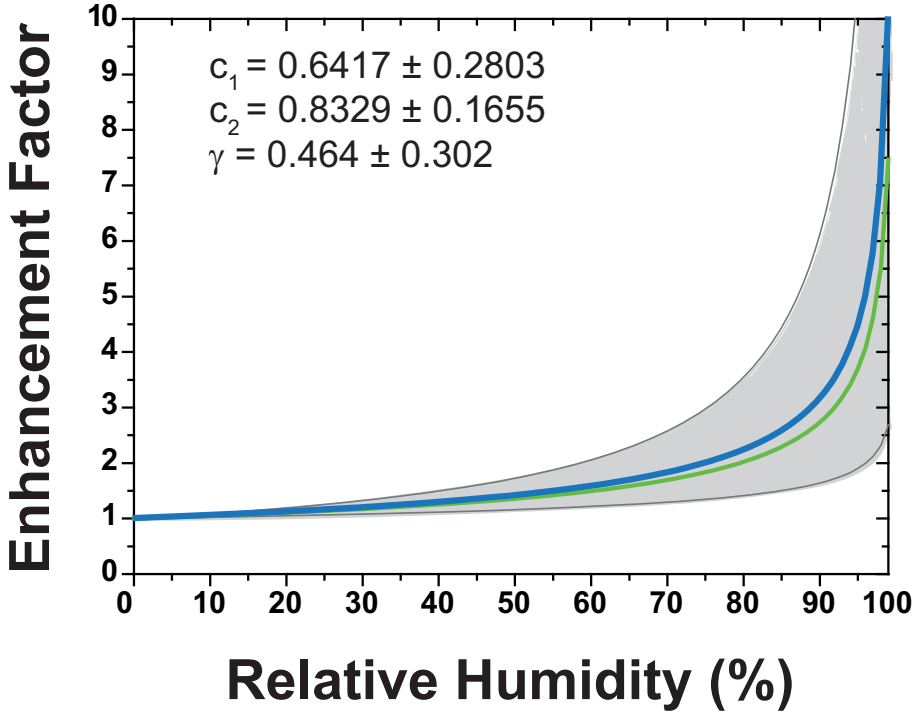

Figure 6. Mean value of the enhancement factor for the 550 nm particle extinction coefficient (blue line, obtained with Eq. (3) for the mean value $\overline{\gamma}$). The upper and lower boundaries of the gray-shaded area are obtained by using $\overline{\gamma} + \delta\gamma$ (upper boundary) and $\overline{\gamma} - \delta\gamma$ (lower boundary) in Eq. (3). The given mean values and SD of the parameters c_1, c_2, and γ result from the evaluation of 143 observational cases collected in the years 2009–2012. The green curve is shown for comparison and represents urban haze conditions after Hänel (1984).

ACPD
15, 12583–12616, 2015

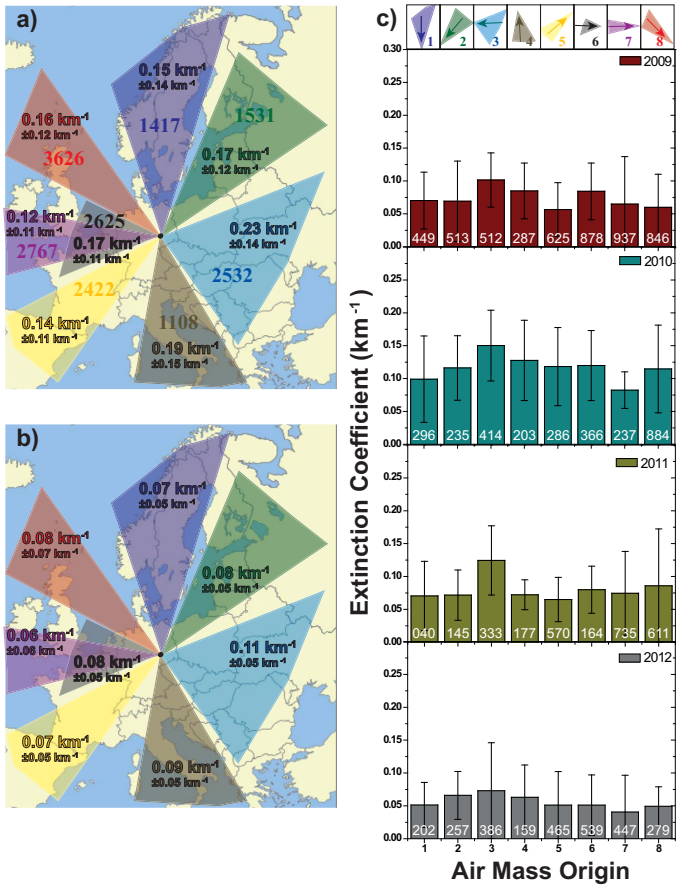

Figure 7. (a) Extinction coefficient (mean value, SD, number of measurements) for eight defined air mass transport regimes based on SÆMS observations from 2009–2012, **(b)** same as **(a)**, except for dry conditions (RH = 0 %), and **(c)** same as **(b)**, but separately for each year of the period from 2009–2012.

ACPD
15, 12583–12616, 2015

Relative-humidity dependence of particle extinction coefficient

A. Skupin et al.

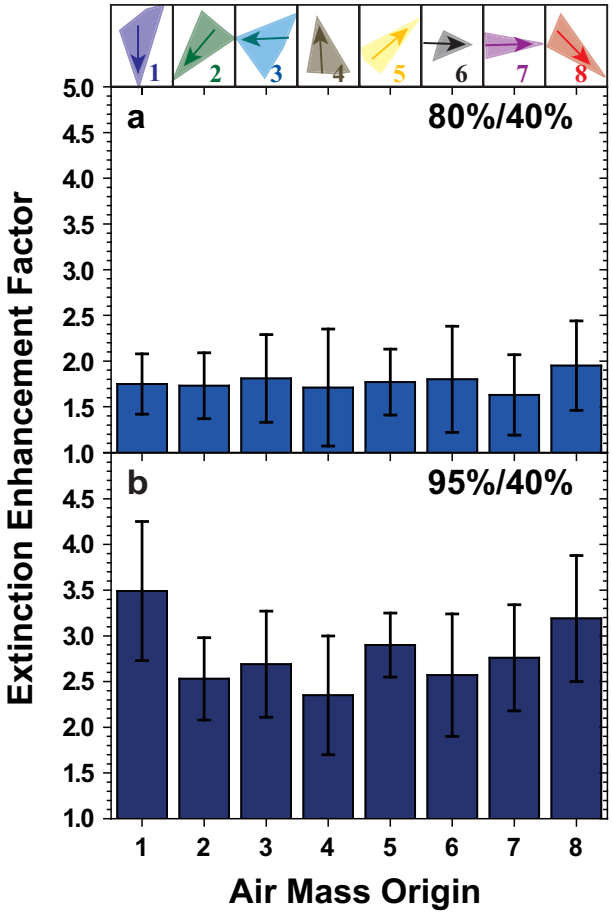

Figure 8. Particle extinction enhancement factor (four-year mean value and SD), for **(a)** 80-to-40 % RH enhancement, and **(b)** 95-to-40 % enhancement for the eight air mass transport regimes.

ACPD
15, 12583–12616, 2015

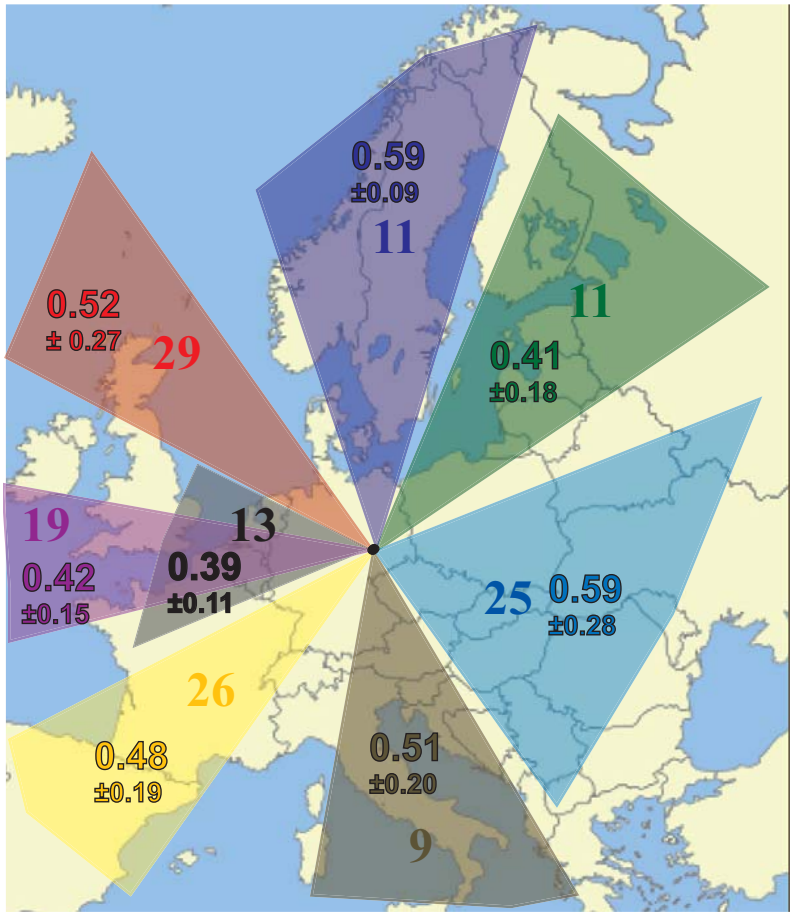

Figure 9. Extinction-enhancement-describing parameter γ (mean value and SD, computed with Eq. 5) for the eight air mass transport regimes derived from SÆMS observations from 2009–2012. Numbers of available cases per cluster are given in addition.

ACPD
15, 12583–12616, 2015

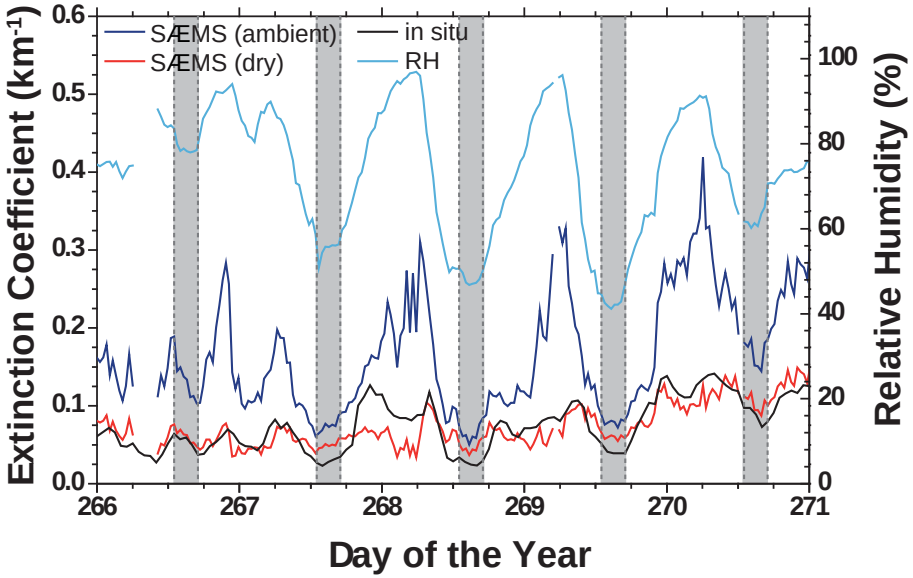

Figure 10. Comparison of 550 nm extinction coefficients measured with SÆMS (ambient, dark blue) and computed from dry particle size distributions (black) measured in situ at the roof of the TROPOS building from 24–29 September 2009. The humidity-corrected SÆMS (dry, 0 % relative humidity) extinction time series is shown as red curve. Relative humidity is given in addition as light blue line. Gray shaded areas indicate the 13:00–17:00 UTC periods during which the PBL is assumed to be well mixed, PBL depth takes its maximum, and relative humidity and particle extinction take their minmum during sunny days (days 267, 268, 269).

ACPD
15, 12583–12616, 2015

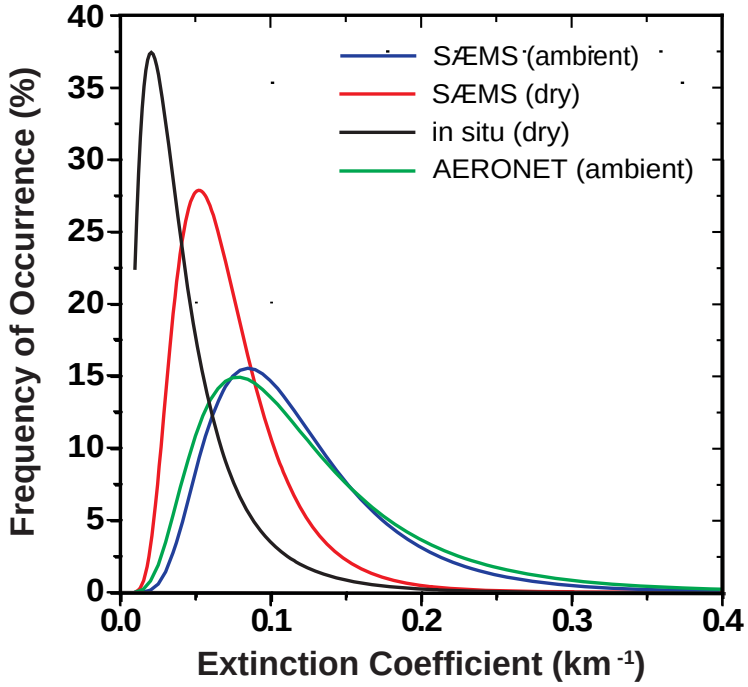

Figure 11. Frequency of occurence of 550 nm particle extinction coefficient measured with SÆMS (ambient) at TROPOS, Leipzig, between 13:00–17:00 UTC of each day in the year of 2009 (blue line). For comparison, the respective distribution for the PBL-mean extinction coefficient (ambient, green) is shown. These values are derived from AERONET sun photometer observations of the 500 nm particle optical depth divided by the PBL depth, which was estimated from GDAS model data. The red SÆMS (dry) curve shows the distribution of humidity-corrected SÆMS 550 nm particle extinction values (for 0 % relative humidity). The black distribution (in situ, dry) shows the 550 nm extinction values calculated from in situ observations of the dry particle size distribution at the roof of the TROPOS building exclusively for the time period from 13:00–17:00 UTC.

ACPD
15, 12583–12616, 2015

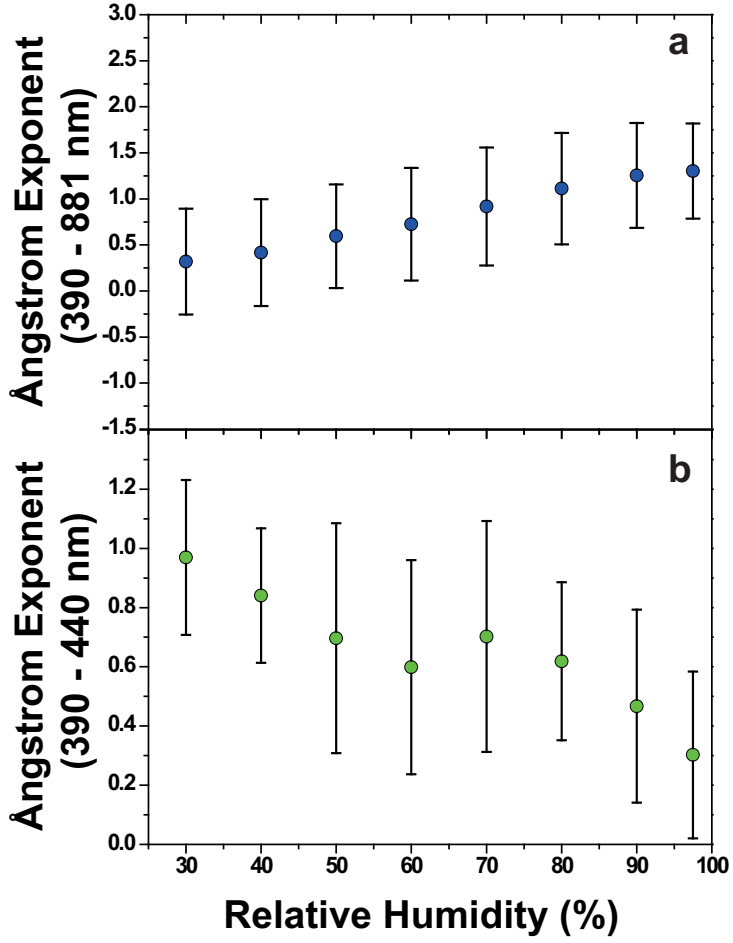

Figure 12. 2009–2010 mean Ångström exponents and SD for the 380–881 nm (top) and 390–440 nm (bottom) wavelength range for eight relative humidity classes.

ACPD
15, 12583–12616, 2015

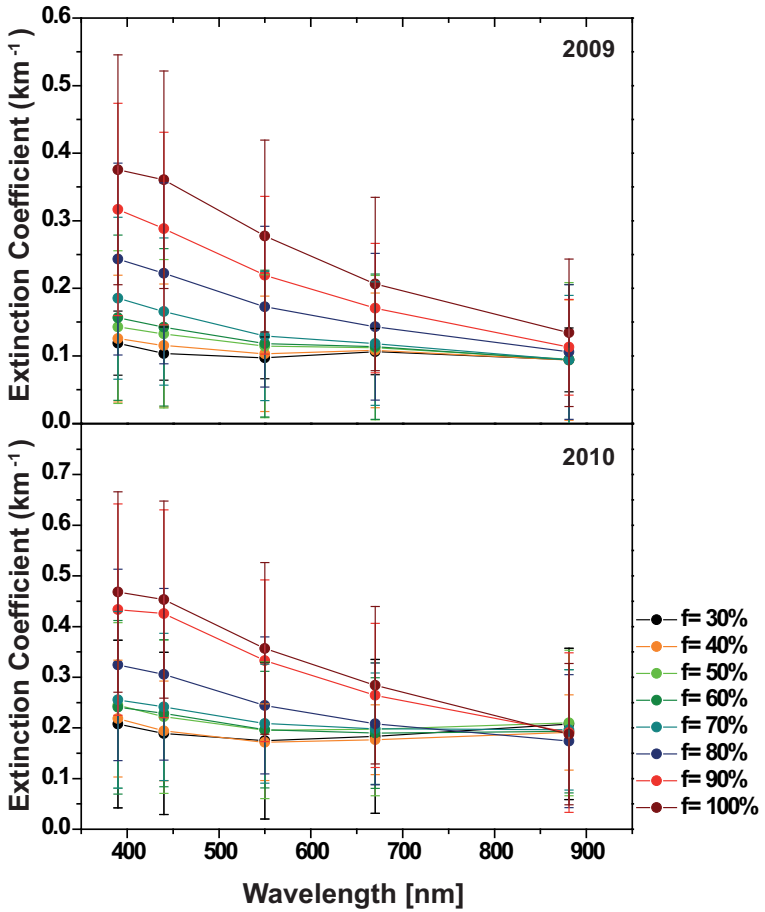

Figure 13. (Top) 2009 and (bottom) 2010 mean extinction coefficient spectrum for eight relative humidity classes (indicated by different colors). Vertical bars indicate the SD for each of the shown five extinction coefficients (for five wavelengths) for a given humidity interval.

ACPD
15, 12583–12616, 2015